THE JOURNAL OF PHYSICAL CHEMISTRY C

Article

pubs.acs.org/JPCC

Optical in Situ Study of InP(100) Surface Chemistry: Dissociative Adsorption of Water and Oxygen

Matthias M. May,*[,†,‡] Hans-Joachim Lewerenz,[§,†] and Thomas Hannappel[∥,†]

[†]Institute for Solar Fuels, Helmholtz-Zentrum Berlin für Materialien und Energie, D-14109 Berlin, Germany

[‡]Department of Physics, Humboldt-Universität zu Berlin, D-12489 Berlin, Germany

[§]Joint Center for Artificial Photosynthesis, California Institute of Technology, Pasadena, California 91125, United States

[∥]Department of Physics, Technische Universität Ilmenau, D-98693 Ilmenau, Germany

Supporting Information

ABSTRACT: Semiconductors designated for solar water-splitting need to be simultaneously stable and efficient in the charge transfer over the interface to the aqueous electrolyte. Although InP(100) has been employed as photocathode for several decades, no experimental data on its initial interaction with water is available. We study reaction mechanisms of well-defined surfaces with water and oxygen employing photoelectron and in situ reflection anisotropy spectroscopy. Our findings show that reaction path and stability differ significantly with atomic surface reconstruction. While the mixed-dimer In-rich surface exhibits dissociative water adsorption featuring In−O−P rather than unfavorable In−O−In bond topologies, the H-terminated, P-rich surface reconstruction is irreversibly removed. Oxygen exposure attacks the In-rich surface more efficiently and additionally modifies, unlike water exposure, bulk-related optical transitions. Hydroxyl is not observed, which suggests a dehydrogenation of adsorbed species already at ambient temperature. Our findings may benefit the design of InP(100) surfaces for photoelectrochemical water splitting.

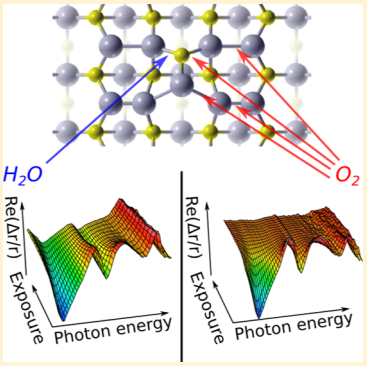

1. INTRODUCTION

Photoelectrochemical water splitting with its product hydrogen is a promising path toward a low-carbon energy system.[1,2] To date, III−V semiconductors such as $Ga_{1-x}In_xP$ enable the highest solar-to-hydrogen efficiencies but are often prone to corrosion in the aqueous electrolyte.[3,4] A detailed understanding of the reactions at the semiconductor−electrolyte phase boundary is desirable to design the semiconductor surface appropriately, reducing corrosion while maintaining an efficient charge transfer over the interface.[5] For GaP surfaces, which were already used in very early approaches for solar water splitting,[6] the conformance of both criteria appears to be challenging because of the formation of an oxide blocking electron extraction.[7] InP(100)-based photocathodes, on the other hand, can be functionalized photoelectrochemically to overcome this difficulty, exhibiting high conversion efficiencies by the formation of a mixture of oxides and phosphates. Currently, the highest efficiencies for this material were obtained starting from the In-rich, (2 × 4) mixed-dimer reconstruction of InP(100) prepared by metal−organic vapor phase epitaxy (MOVPE).[8,9]

The interaction of water and oxygen with GaP and InP surfaces was recently the subject of several computational studies proposing reaction paths and molecular dynamics at different surfaces.[5,10−12] Strained In−O−In bonds, for example, were proposed to create hole traps leading to corrosion.[10] While the in situ access to the semiconductor−liquid interface at sufficient surface sensitivity in an electrolyte is experimentally rather difficult, gas-phase adsorption experiments in ultrahigh vacuum (UHV) constitute a possibility for bridging the gap between liquid environments and very well-defined surfaces in UHV. Such experiments typically combine water adsorption with ultraviolet or X-ray photoelectron spectroscopy (UPS/XPS) prior to and after exposure and identify the chemical species formed.[13−17] Recently, also ambient-pressure XPS was utilized to study III−V surfaces.[18] When differently reconstructed surfaces were employed, it was shown that the surface chemistry of the specific surfaces differs significantly.[15−17] III-rich surfaces appear to be typically much more reactive than the P-rich, H-passivated surfaces.[15,17] For a microscopic understanding of the surface chemistry, very clean and well-defined surfaces are an essential prerequisite as surface contamination by, for example, carbon, significantly impacts surface reactivity.[17]

In this paper, we study the interaction of oxygen and water with the mixed-dimer, (2 × 4) reconstructed In-rich surface as well as the P-rich $p(2 \times 2)/c(4 \times 2)$ surface (see Figure 1; in the following, termed "In-rich" and "P-rich", respectively) of InP(100) with complementary spectroscopic methods. Reflection anisotropy spectroscopy allows us to study morpho-

Received: March 25, 2014
Revised: July 30, 2014
Published: July 30, 2014

   dx.doi.org/10.1021/jp502955m | J. Phys. Chem. C 2014, 118, 19032−19041

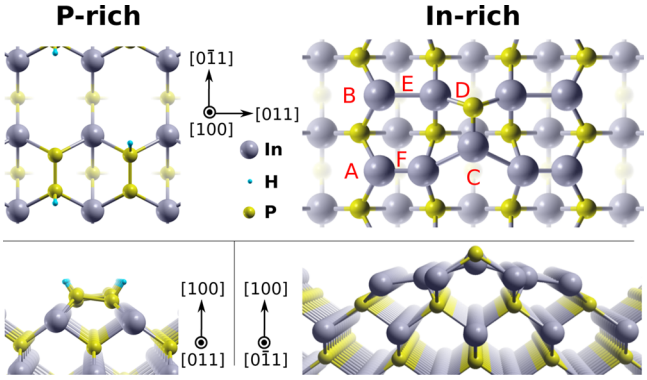

Figure 1. Ball-and-stick sketch of the considered surface reconstructions of InP(100).[19,20] The left-hand side shows the P-rich $p(2 \times 2)/c(4 \times 2)$ reconstruction, the right-hand side the In-rich, (2×4) mixed-dimer reconstruction. Potential adsorption sites on the In-rich surface are labeled A–F.

logic changes of the surface in situ during adsorption and thermally activated desorption. Photoelectron spectroscopy, applied *in system*, enables us to probe changes of the electronic structure induced by the adsorbates and to benchmark the corresponding optical in situ signals. Regarding surface ordering and oxygen incorporation into the surface, we find that the P-rich surface is less stable against water than oxygen exposure, while the situation is reversed for In-rich surfaces. The surface interaction of both adsorbates with the In-rich surface, however, appears to exhibit a high degree of reversibility. By identifying potential reaction paths, our findings could improve the understanding why initially In-rich InP(100) photocathodes perform so well in water-splitting applications. Exploiting the reactivity of the In-rich surface in a controlled manner can facilitate surface transformations into an InP/n-InPO_x structure, promoting charge transfer to the electrolyte over a stable interface film.

2. EXPERIMENTAL DETAILS

Reflection anisotropy spectroscopy (RAS) is an optical, highly surface-sensitive tool that can be applied in situ in UHV, during metal–organic vapor phase epitaxy in gas ambient, as well as at the solid–liquid interface.[21−23] In particular, the latter feature is very promising for applications in semiconductor electrochemistry: While the surface sensitivity is sometimes even higher than UPS,[17] as in the case of an optically isotropic bulk, the signal originates only from the first atomic layer; it is not restricted by the low mean-free path of probes such as electrons at ambient pressures. RAS enables us to access the InP surface in situ during growth, adsorption of H_2O/O_2, as well as thermal desorption. A future application together with ambient pressure XPS could be a very powerful combination for probing surface chemistry in situ.

For RAS, linearly polarized light impinges on a sample and the difference in reflection of two perpendicular axes is detected:

$$\frac{\Delta r}{r} = 2\frac{r_{[0\bar{1}1]} - r_{[011]}}{r_{[0\bar{1}1]} + r_{[011]}}, \quad r \in \mathbb{C} \tag{1}$$

In the case here, the two perpendicular axes are the [011] and the [0$\bar{1}$1] direction of the (100) surface. We will consider only the real part, Re($\Delta r/r$), in the following.

The principle of RAS is sketched in Figure 2 for the case of two dimerized (100) surfaces, as can be found, for example, for

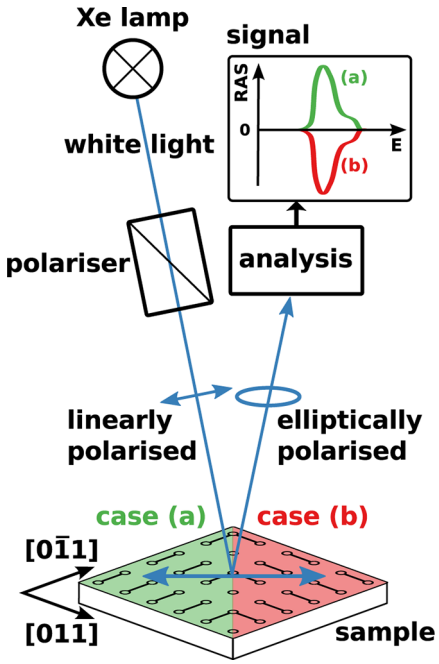

Figure 2. Principle of RAS. White, polarized light impinges at near-normal incidence onto a sample. If an optical anisotropy exists, the reflected light is elliptically polarized and analyzed as a function of energy.[24] Case (a) shows a dimerized surface with the dimer orientation along the [0$\bar{1}$1]-direction (green). Case (b) shows the same surface with a perpendicular dimer orientation along the [011]-direction (red), leading to a reversed sign of the RAS signal.

H-terminated Si(100).[21] The dimers exhibit an optical transition along their axis leading to an optical anisotropy of the surface. Here, the only difference between surfaces (a) and (b) is the orientation of the dimers, leading to a reversed sign of the resulting RAS signal of the surface (assuming no bulk contribution). If both dimer orientations are present within the analysis region, the signals are superimposed, leading to a zero line in the case of a 1:1 ratio of both dimer orientations.[21]

Detailed electronic structure and RA spectra calculations correlated spectral features of the InP(100) surface with optical transitions between specific electronic states,[19,20,25] allowing for the identification of the origin of spectral modifications and a quantitative interpretation.[26] We employed a commercial LayTec EpiRAS 200 spectrometer in our experiments; zero-line effects were accounted for by the use of an optically isotropic Si(100) reference sample.

Homoepitaxial, not intentionally doped InP(100) was grown on p-doped InP(100) wafers in the process gas hydrogen applying the precursors *tert*-butylphosphine (TBP) and trimethylindium in an Aixtron AIX200 reactor modified to enable a contamination-free transfer to UHV.[27] The application of RAS during growth allows for the specific preparation of the In- or the P-rich surface already in the reactor.[22,26]

After contamination-free transfer from MOVPE ambient to UHV, samples were first characterized by PES, followed by exposure to H_2O or O_2 at room temperature and pressures in the order of 10^{-5} mbar in an adjacent UHV chamber. The chamber is equipped with an optical viewport to enable in situ RAS during exposure; the pressure for the determination of the

dx.doi.org/10.1021/jp502955m | J. Phys. Chem. C 2014, 118, 19032−19041

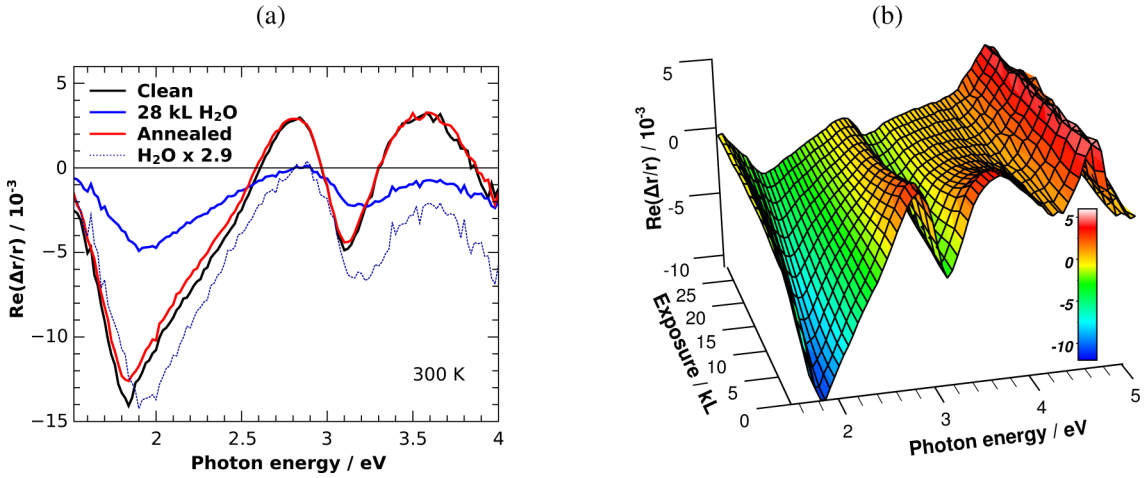

Figure 3. (a) RA spectra of initially In-rich, (2 × 4) InP(100) before exposure to H_2O (black), after exposure (blue), and after annealing in H_2 to 570 K (red). The blue, dashed line shows the spectrum after exposure scaled by a factor of 2.9. (b) Time-resolved evolution of the RA spectrum during water exposure.

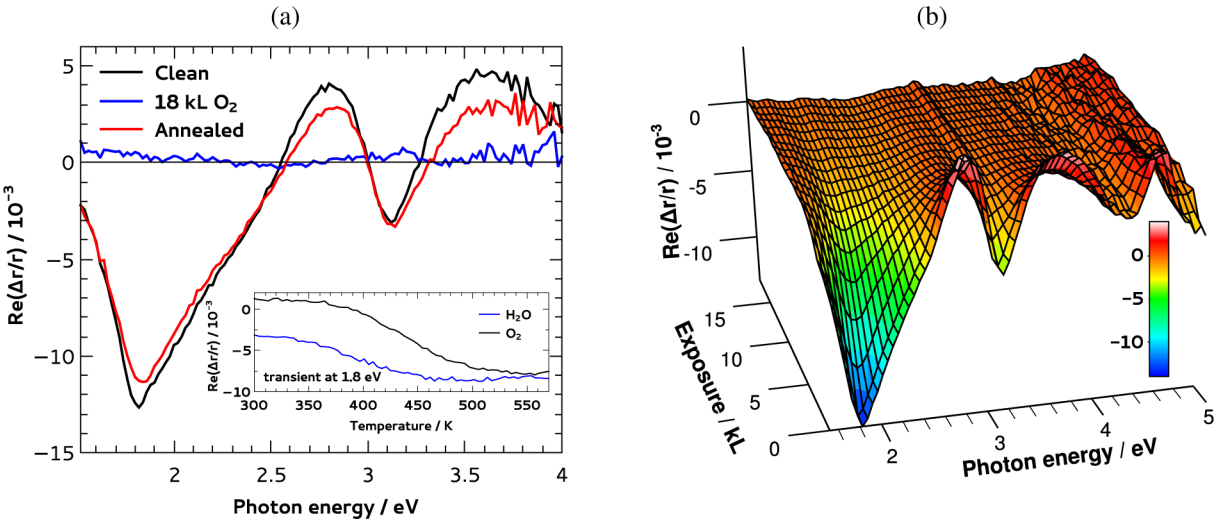

Figure 4. (a) RA spectra of the In-rich InP(100) surface before (black) and after (blue) exposure to O_2 and after annealing in H_2 to 570 K (red). Inset shows the RAS transients at 1.8 eV of H_2O/O_2 exposed surfaces during annealing. (b) Time-resolved evolution of the RA spectrum during oxygen exposure.

exposure was measured with a cold cathode.[17] Here, exposure was quantified in langmuir (L), where 1 L = 1 Torr × 1 μs would correspond to one monolayer, if the sticking coefficient was unity. After a second characterization with PES, samples were transferred back to the MOVPE reactor via UHV and annealed in ultrapure hydrogen, again with RAS control. Finally, samples were once more analyzed with PES. For X-ray or ultraviolet photoelectron spectroscopy (XPS/UPS), we used a Specs Phoibos 100 analyzer in combination with a monochromated Al Kα source (Specs Focus 500) or a He gas discharge lamp, respectively. The energy scale was calibrated with a sputtered Au reference sample, and for XPS, samples were tilted 60° against normal emission to increase surface sensitivity.

3. RESULTS

3.1. In-Rich, Mixed-Dimer Surface. The surface chemistry of In-rich surfaces has already been the subject of several computational studies and it has proven to be a well-suited starting point for water-splitting photocathodes.[5,8,10,12] Typical for MOVPE preparation, this surface is characterized by a mixed-dimer consisting of a phosphorus and an indium atom followed by a layer of In atoms with In−In bonds in the [011]-direction (see Figure 1). First, we will discuss the origin of relevant RAS features and compare water and oxygen exposure with respect to RAS. This will be followed by valence-band photoelectron spectroscopy and finally X-ray photoelectron spectroscopy of the relevant core levels.

3.1.1. Optical Spectroscopy. RA spectra of an In-rich sample are shown in Figure 3. The electronic structure of the surface giving rise to the distinct features of the RA spectrum was studied in great detail in the literature.[19,28−31] The strong negative feature of the clean surface between 1.5 and 2.5 eV is most sensitive to surface chemistry and related to the specific surface reconstruction.[29,32] The higher-energy part of the RA spectrum beyond 2.5 eV is mainly ascribed to surface-modified bulk transitions: the critical point energy of the bulk transition near E_1 is around 3.2 eV, $E_0^{'}$ around 4.8 eV.[25,30,33]

The major contribution around 1.8 eV of the asymmetric surface feature is closely related to In−In bonds along the

dx.doi.org/10.1021/jp502955m | J. Phys. Chem. C 2014, 118, 19032−19041

[011] direction (A, C, and F in Figure 1). It arises from a transition from an occupied σ-like surface state V_1 (notation from ref 28) between the top In atom and the second atomic layer consisting of In atoms (near site C in Figure 1) to an unoccupied surface state C_3 consisting of dangling In bonds (sites A, C, F).[19,29] Consequently, this feature is very sensitive to chemisorption involving the dangling In bonds. The second-largest contribution to the negative feature at slightly higher energies stems from the occupied surface state V_3, also related to the In−In bonds, but with its wave function more localized between the two In atoms at the P side of the dimer (site E). Its counterpart, the unoccupied state C_1, is again originating from dangling In bonds, but is more localized at the mixed-dimer (site D).[19] As these exact bond topologies play a prominent role in the surface chemistry studied computationally by Wood et al.,[12] RAS is an excellent tool for probing the proposed surface reactions. The contribution of the mixed-dimer itself, i.e., the top In−P bond, to the RA spectrum is comparably small. In terms of energy, the occupied surface states involved in the origin of the RA spectrum are located slightly below the valence band maximum and hence are also accessible to photoelectron spectroscopy.

The pristine InP surface was exposed to H_2O vapor under continuous in situ RAS control until the RA spectrum did not significantly change over time (Figure 3b). After 28 kL of H_2O exposure, all spectral features are greatly reduced, but do not vanish completely, as one would expect for a completely disordered surface. This is still the case for exposures up to 100 kL (not shown here). We also observe a general blue-shift of the spectrum (see upscaled spectrum in Figure 3), which could be due to a surface dipole inducing a linear electro-optic effect.[17,34] The overall, more or less symmetrical reduction of the spectrum points toward an attack of both the In−In bonds and In−P bonds. Regarding the bulk-related features in the RA spectrum, the transition E_1 at 3.2 eV appears to be affected by the water exposure, while the higher-energy feature (4.6 eV) near the $E_0^{|}$ transition is not (see Figure 3b).

To evaluate, whether the observed behavior is specific for water, we also exposed the In-rich surface to molecular oxygen (Figure 4). Unlike for water exposure, this results in basically a zero line of the RA spectrum, as observed in the literature,[15] but with a small, reproducible, positive feature at 3.2 eV near the critical point transition E_1 (Figure 4a). The flat spectrum at higher energies, where the surface-modified bulk transitions E_1 and $E_0^{|}$ are located, suggests an attack of the In backbonds, i.e., a diffusion of the oxygen toward the bulk.

As a measure for the reactivity, we define the mean lifetime τ of the negative anisotropy at 1.8 eV assuming a mono-exponential decay. The time-resolved evolution of the RA spectrum can be extracted from the in situ RA measurement during exposure. For exposure pressures in the range of 10^{-5} mbar H_2O, the lifetime is in the range of τ_{H_2O} = 15−20 kL. (Because of slow reaction kinetics, τ actually depends on the exposure pressure.) The mean lifetime for oxygen exposure, on the other hand, is with $\tau_{O_2} \approx 2.8$ kL (at 2×10^{-5} mbar) significantly smaller than for H_2O, indicating a higher reactivity of the surface toward oxygen exposure. In the cases where small amounts of carbon were detected on the surface by XPS prior to exposure because of limited UHV conditions or residual precursors from growth, the lifetime was reduced by a factor of 2. Those samples are not considered further here.

RAS also allows a time-resolved monitoring of the exposed surface during annealing to probe reversibility and desorption temperature. Annealing of the water-exposed surface in hydrogen can completely restore the RA spectrum (Figure 3a). This reconstitution of the surface after H_2O exposure occurs at very modest temperatures around 380 K (minimum of derivative), as evidenced by the reappearance of the related RAS feature at 1.8 eV (inset of Figure 4a). This is in stark contrast to the structurally very closely related III-rich surface of GaP(100), where even annealing at 680 K cannot completely restore the surface reconstruction.[17] The low temperature and the high degree of reversibility suggest that only the top bonds of the surface, and not the backbonds, are attacked by the water molecules in a reversible manner, which is a favorable behavior regarding stability. For the oxygen-exposed surface, the RA spectrum is restored to a slightly lower degree (especially at the higher energies where the spectrum originates from surface-modified bulk transitions) and at higher temperatures: The minimum of the derivative of the RAS transient in Figure 4a is located around 450 K. The applied maximum temperature of 570 K is still well below the typical deoxidation temperature of 870 K for an InP wafer prior to growth.

To summarize, RAS shows that the reactivity of the In-rich surface for O_2 is significantly higher than that for H_2O exposure. Oxygen induces an almost flat spectrum, i.e., an optically isotropic surface. After water exposure, on the other hand, the optical anisotropy is partly conserved for the optical transitions related to the surface reconstruction and almost completely for the surface-modified bulk transition $E_0^{|}$. Annealing of the surface under RAS control shows a facile reconstitution of the water-exposed surface, while the impact of oxygen is more persistent.

3.1.2. Photoelectron Spectroscopy. To probe the influence of the adsorbate on the valence band electronic structure, we performed ultraviolet photoelectron spectroscopy, which constitutes a well-suited complementary technique at a similar surface sensitivity. Spectra of a single sample at different stages of the H_2O adsorption experiment acquired with the He II excitation are presented in Figure 5. The peak around E_B = 0.75

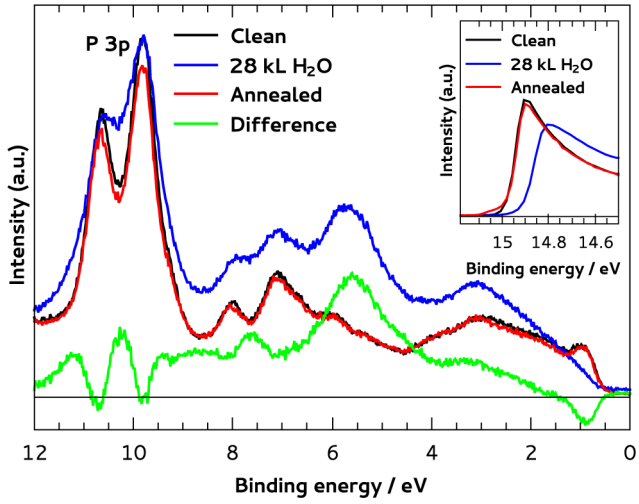

Figure 5. He II ($h\nu$ = 40.82 eV) photoelectron spectra of the In-rich surface before exposure to H_2O (black), after exposure (blue), their difference (green), and after annealing in H_2 to 570 K (red). Inset shows the secondary electron cutoffs (measured with He I). Binding energies are referenced to the Fermi level.

dx.doi.org/10.1021/jp502955m | J. Phys. Chem. C 2014, 118, 19032−19041

eV of the clean surface (black curve) near the valence band maximum originates from the occupied surface state V_1[19,31] and disappears after water exposure. The quenching of the occupied surface state V_1 evidences an interaction of water at the cation site (C in Figure 1) of the mixed-dimer. An insertion into the dimer itself appears unlikely because the RAS signature would not be affected to that extent by the modification of its In−P bond. At this location, Wood et al. expect dissociative adsorption with the phosphorus atom acting as the Lewis base and the indium atom as the Lewis acid hosting a hydroxyl.[12] They do, however, suggest that molecular adsorption at the outermost In atoms in this row is slightly more favorable. While molecular adsorption is necessarily the very first step of the following reaction, we could not identify its typical signature with UPS in our static view after exposure. The hypothesis of the dimer being involved in the adsorption process is also supported by the modification of the P 3p emission if we assume that the water attacks only the very surface as supported by the complete recovery of the RA spectrum after annealing. The next phosphorus atoms are located below the first layer of In atoms.

Apart from the modification of P 3p and the surface state, the additional, water-induced states displayed by the difference spectrum (green curve) exhibit a strong and broad peak around 5.6 eV binding energy (5 eV below the valence band maximum (VBM)), originating most probably from the O 2p level, and a less intense peak around 7.6 eV (7 eV below VBM).

The exact reconstitution of the PE spectrum after annealing is in agreement with the findings for RAS and again underlines the reversibility of the process.

He II photoelectron spectra of the oxygen-exposed surface largely resemble the signal after water exposure, but with a small, additional peak in the difference spectrum at 9 eV and a significantly higher, additional intensity between 4 and 6 eV, which we assign to O 2p states. The surface state-related contribution near the valence band maximum again disappears after exposure and can be restored after annealing, with only some intensity missing, similar to the negative anisotropy of the RA spectrum. At larger binding energies in the range of the O 2p emission, however, the spectrum displays additional electronic states. This suggests, in agreement with the reduction of the surface-modified bulk transitions of the RA spectrum, diffusion of the oxygen toward the bulk with the surface structure being largely reconstituted.

A significant difference between the two adsorbates is their influence on the work function: While for water exposure the secondary electron cutoff (inset of Figure 5) is shifted about 70 meV to higher kinetic (lower binding) energies, the shift after oxygen exposure is ca. 310 meV (inset of Figure 6). As we could not detect a significant shift of binding energies, the difference in work function stems from a surface dipole. A surface dipole enhancement would agree well with the formation of In−O−In bridges.[12] Also, for the dipole, the water-exposed surface exhibits a higher degree of reversibility.

X-ray photoelectron spectroscopy (XPS) provides an insight into the chemical environment of oxygen. A monochromated Al Kα source was employed, and samples were tilted 60° against normal emission to increase surface sensitivity; the signals originating from the oxygen located at the very surface are small at the applied excitation energy. Peak fitting of Voigt profiles and a linear background was performed using fityk.[35] For water exposure, the spectrum around the O 1s line (Figure 7a) after exposure mainly exhibits two contributions, O_I at

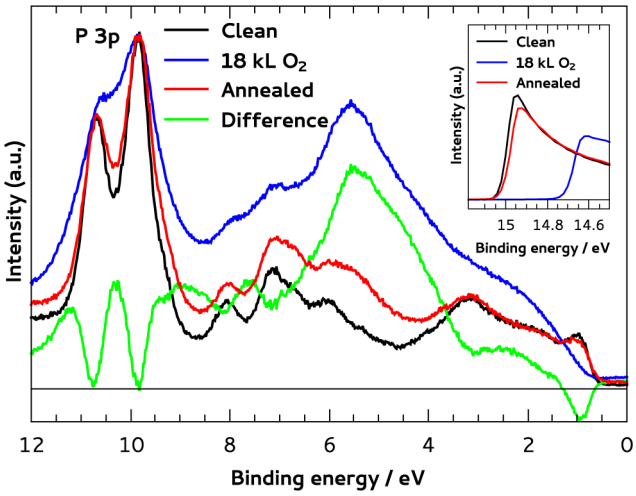

Figure 6. He II ($h\nu$ = 40.82 eV) photoelectron spectra of the In-rich surface before exposure to O_2 (black), after exposure (blue), their difference (green), and after annealing in H_2 to 570 K (red). Inset shows the secondary electron cutoffs (measured with He I).

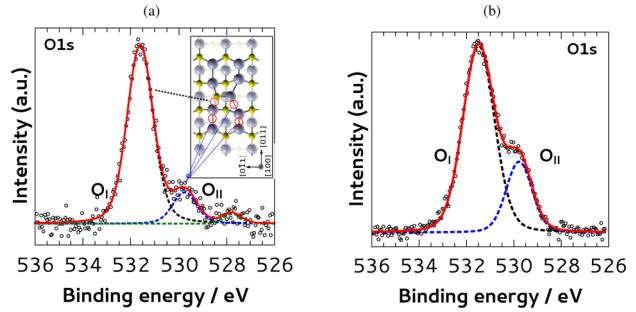

Figure 7. X-ray photoelectron spectra (mon. Al Kα; takeoff-angle, 30°) of the In-rich surface after exposure to water (a) and oxygen (b).

531.6(±0.2) and O_{II} at 529.8(±0.2) eV with a very weak, additional contribution at 527.8(±0.3) eV. These former two contributions fit quite well to the two types of oxygen O^{2-} ions found in In_2O_3 (reported splitting: 1.6 eV),[36] suggesting a surface oxide similar to In_2O_3. The latter, very weak contribution (green curve in Figure 7a) could be oxygen bound to surface defects. The oxygen contribution of molecular H_2O, which would be expected around 533 eV,[17,37] does not appear to be present. A potential, very weak contribution of OH^-, expected around 532 eV, is possibly not resolved because of the tails of the stronger oxide emission but appears to be unlikely because the peak after oxygen exposure (see below) is located at the same position. In single-crystal In_2O_3, O_I is attributed to oxygen-deficient regions and exhibits a third of the intensity of O_{II}.[36] We find an opposite ratio of about 6:1, which could be due to the presence of phosphorus, with only a minority of the oxygen in an In−O−In configuration. Chen et al. assign O_I around 531.5 eV to In−O−P bonds, pointing toward an oxygen insertion at site D, and ascribe a second feature at 530.1 eV to In−O−In bonds.[15] Therefore, the oxygen binding to the surface after dissociative water adsorption is to the largest part inserted near the phosphorus atom of the mixed-dimer (site D).

The O 1s signal after oxygen exposure shows two contributions; again, one at 531.5(±0.2) eV and the second at 529.8(±0.2) eV (Figure 7b). The peak ratio of O_I:O_{II} ≈ 3:1 is about half of the ratio found after water exposure, but their

dx.doi.org/10.1021/jp502955m | J. Phys. Chem. C 2014, 118, 19032−19041

location coincides quite well. Therefore, a hydroxyl group decoration as an origin of O_I in the case of water exposure appears to be unlikely, favoring the In−O−P scenario for water exposure and a higher tendency to form In−O−In bonds for oxygen interacting with the surface.

Following the conventional formalism of XPS,[38] we estimated the fractional overlayer coverage (q) as

$$q = -\frac{I}{\exp[-d/\lambda_o(E_o)\cos\theta] + I\exp[-d/\lambda_o(E_s)\cos\theta] - I - 1} \quad (2)$$

with the overlayer thickness d (calculated from bulk water), the electron attenuation length (EAL) of the overlayer λ_o, the kinetic energies of substrate (In 3d) and overlayer (O 1s) E_s and E_o, respectively, and the angle θ against normal emission. The term $I = I_{o,rel}/I_{s,rel}$ was defined via the ratio $I_{o,s,rel} = I_{o,s}/I^{\infty}_{o,s}$ of measured intensity $I_{o,s}$ against the calculated intensity of an infinitely thick layer $I^{\infty}_{o,s}$. EALs were calculated with the NIST database[39] with the number of valence electrons for water N_v = 8 and a band gap of 6.9 eV;[40] photoelectron ionization cross sections were taken from Yeh and Lindau.[41]

In the case of water exposure, this results for the In-rich surface in a coverage of 0.22(±0.1) monolayers (ML). For oxygen, the relative intensity I for O 1s is 2.5 times higher than that for water, but the quantification in terms of monolayer fraction is more problematic because of structural uncertainties such as potential bulk diffusion mentioned above.

XPS of In 3d core levels does not reveal any changes due to the limited surface sensitivity associated with the Al Kα source, but the He II excitation energy enables the probing of the In 4d core level at very high surface sensitivity (kinetic energy in the order of 23 eV). The upper part of Figure 8a shows the core level before water exposure, with the red (17.33 and 18.21 eV binding energy) lines corresponding to bulk states and the blue and green lines (16.86, 17.73 eV and 17.60 and 18.47 eV) to surface core level shifts, respectively. After water exposure, the contribution around the second surface core level (green, 17.82 and 18.68 eV) is increased, stemming from the oxide species mentioned above. The weaker surface core level shift, located at a very similar energy, could not be resolved any longer. After the sample was annealed, the In 4d core level spectrum is reconstituted to its original state (not shown here). Oxygen (Figure 8b), on the other hand, leads essentially to the same oxide species (17.84 and 18.68 eV). After the sample was annealed, the oxide species is still present with a slight shift (17.68 and 18.56 eV) in the direction of the original core level shift and a small, additional contribution (orange) at 17.39 eV, with the second component of the doublet not resolved. A quantitative comparison can be made by subtracting the intensity of the second surface core level shift contribution from the oxide species and setting the remaining signal in relation to the bulk intensity. While the ratio of bulk to oxide species is 50:1 after water exposure, we observe a ratio of 6:1 after oxygen exposure, corresponding to the different signal intensities of the O 1s species assigned to In−O−In bonds (see Figure 7).

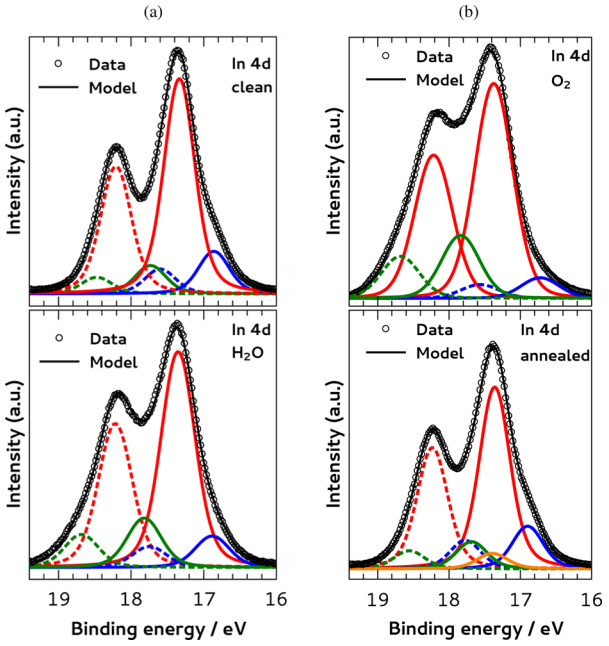

Figure 8. He II photoelectron spectra of the In 4d core level of the In-rich surface (a) before and after exposure to water and (b) after exposure to oxygen and annealed after oxygen exposure. Colored lines are the deconvoluted components; solid and dashed lines correspond to the respective spin−orbit doublets.

In summary, PES reveals the oxygen bond topology formed after both water and oxygen exposure, which is mainly of an In−O−P character. Oxygen exposure does, however, show an increased tendency to form In−O−In bonds. Resulting saturation coverages are in the submonolayer range with approximately two (four) oxygen atoms per surface unit cell for water (oxygen) exposure. While annealing can completely restore the water-exposed surface, this is not the case for oxygen exposure with oxygen probably diffusing toward the bulk. Signatures of OH^- were not found, indicating a dissociative adsorption of water releasing both hydrogen atoms of the water molecule.

3.2. P-Rich Surface. The P-rich surface is the second main surface reconstruction that is typical for MOVPE growth of InP(100), but unlike the In-rich surface, its initial water−oxygen interaction has not been studied computationally. Its surface is characterized by two oppositely buckled P-dimers, which are stabilized by a hydrogen atom (see Figure 1). The same configuration can also be found for GaP(100) surfaces, where it exhibits an extraordinary stability against water exposure.[17] Unlike the In-rich surface, the $(2 \times 2)/c(4 \times 2)$ P-rich surface cannot be prepared in UHV via an annealing procedure only, but with supply of hydrogen.[20] In MOVPE ambient, the H-terminated surface can be obtained by cooling the sample after growth to 570 K under TBP supply and subsequent annealing to 630 K with RAS in situ control to remove residual precursors.[26]

The most characteristic feature of the RA spectrum (Figure 9) is the strong negative anisotropy around 1.85 eV, which becomes extremely sharp at low temperatures and originates from P−H bonds, followed by a strong positive feature in the region of 3.1 eV.[20,31]

After water exposure, the characteristics of the RA spectrum disappear and are replaced by a very broad and weak negative anisotropy between 1.5 and 3.2 eV. The lifetime τ_{H_2O} of the surface ordering measured by RAS is, for exposure pressures in the 10^{-5} mbar range, with 7−13 kL about half of the lifetime of the In-rich surface for H_2O. Although at first surprising, as the analogue V-rich surface of GaP(100) exhibits a significantly higher stability of the RA spectrum,[17] this is in agreement with the fact that the P-rich surface of InP develops, in comparison

dx.doi.org/10.1021/jp502955m | J. Phys. Chem. C 2014, 118, 19032−19041

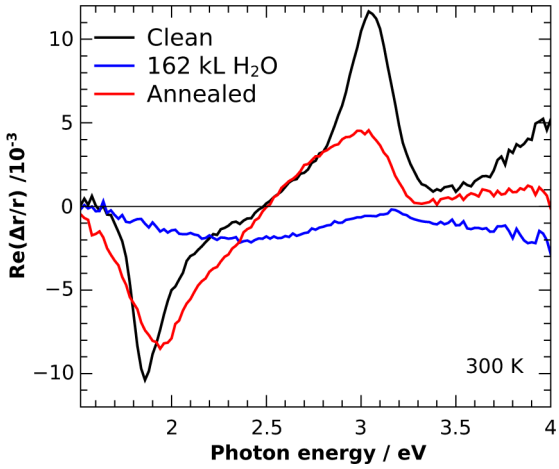

Figure 9. RA spectra of initially P-rich, $p(2 \times 2)/c(4 \times 2)$ InP(100) before exposure to water (black), after exposure (blue), and after annealing in H_2 to 570 K (red).

to P-rich GaP, at much lower temperatures (638 versus 750 K) a preferential desorption of phosphorus.[22,26,42,43] After the sample is annealed to 570 K, which is well below the temperatures of preparation and preferential phosphorus desorption, the exposed surface changes toward an In-rich RA spectrum (Figure 9). This suggests that water destabilizes the P-dimer, facilitating surface phosphorus desorption. The destabilization could be due to a removal of the stabilizing hydrogen atom.[17] A destabilization by permanent insertion of oxygen into the surface can be ruled out, as the resulting oxygen coverage after exposure evidenced by XPS is very low, i.e. 0.08(±0.04) ML, even after 162 kL, which corresponds to ~12τ. One oxygen atom per P dimer would correspond to 0.5 ML.

XPS in the O 1s region after water exposure (Figure 10a) reveals one major peak at 531.5(±0.2) eV as a common feature

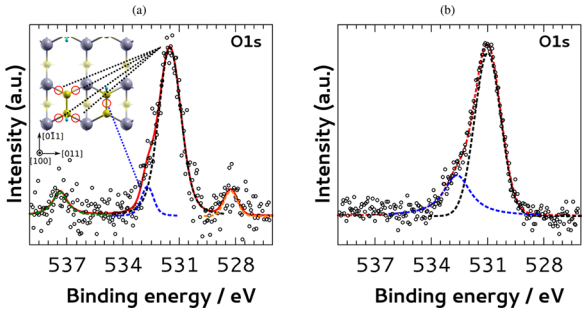

Figure 10. X-ray photoelectron spectra (mon. Al Kα; takeoff-angle, 30°) of the P-rich surface after exposure to water (a) and oxygen (b).

with the O 1s spectra of the In-rich surface attributed to In−O−P bonds (see above). Three minor contributions at 537.5(±0.2), 532.7(±0.25), and 528.2(±0.3) eV appear as well. While the former features are unique for H_2O exposure of the P-rich surface, the latter feature around 528 eV is common to both surfaces and could be a subsurface oxygen species. The feature at 532.7 eV could originate from molecular water or phosphate species.[44] The origin of the very weak O 1s signal at 537.5 eV is difficult to assign. Lundholm et al. assign a similar binding energy to liquid H_2O in LiCl.[45] The feature could possibly arise from water molecules stabilized by the P-dimer with a hydrogen bond or oxygen bound to a phosphorus-releated surface defect. Gas-phase water can be ruled out with a pressure in the analysis chamber in the low 10^{-10} mbar range. For an oxygen exposure of 33 kL (Figure 10b), the overall O 1s signal is again significantly stronger and the relative oxygen intensity I is 2.5 times higher than that for water exposure. Here, only two oxygen peaks can be identified at 532.6(±0.3) and 531.0(±0.2) eV. The former peak coincides with the oxygen species found after water exposure, suggesting that both indeed stem from phosphate species or rather P−O−P bonds and not from molecular water.[15] The signal at 531 eV could be the ubiquitous O_I species, albeit at higher binding energy, possibly induced by local strain.

The RA spectrum of the oxygen-exposed surface (Figure 11) is, again in contrast that of to the In-rich surface, more

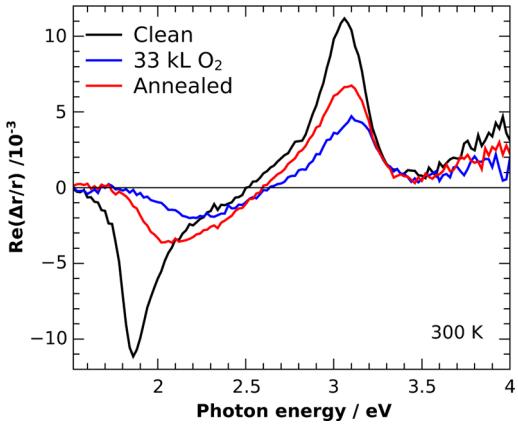

Figure 11. RA spectra of initially P-rich, $p(2 \times 2)/c(4 \times 2)$ InP(100) before exposure to oxygen (black), after exposure (blue), and after annealing in H_2 to 570 K (red).

structured than the spectrum of the water-exposed surface. It has lost most of its original intensity, apart from the low-energy negative anisotropy related to P−H bonds below 2 eV, which completely disappears. Annealing restores part of the original intensity, but not the P−H related peak. A transition toward In-rich, i.e., a loss of phosphorus, is also not observed, as evidenced by the characteristic positive anisotropy around 3.1 eV.

4. DISCUSSION

With the findings outlined above, we can formulate potential reaction paths dominating the initial interaction of water and oxygen with the In-rich surface (eqs 3 and 4). Water exposure is clearly dissociative, as no evidence for molecular water on the surface was found. Hydroxyl groups are necessarily an intermediate species of this process but do not appear to be present on the surface after exposure, as supported by a direct comparison with oxygen exposure, lacking a source of hydrogen. Instead, our findings suggest that the product is rather mainly oxygen covalently bound near the phosphorus atom of the mixed-dimer (site D in Figure 1) as evidenced by RAS and UPS. This is in contrast to low-temperature water adsorption on UHV-cleaved InP(110) surfaces, in which no O−P topologies were found.[14] With a different surface and higher temperature during adsorption, however, the comparability to our results is limited. However, ambient-pressure XPS studies of GaAs(100) surfaces, a similar III−V semiconductor system, do find hydroxyl only up to 200 K with a

dx.doi.org/10.1021/jp502955m | J. Phys. Chem. C 2014, 118, 19032−19041

dehydrogenation at higher temperatures. As we study water adsorption at 300 K, the dehydrogenation process is already invoked during exposure.

The resulting coverage of approximately a quarter of a monolayer corresponds to two oxygen atoms per surface unit cell with only a small fraction exhibiting the In−O−In signature. Therefore the oxygen could be symmetrically inserted as In−O−P at site D, releasing two hydrogen molecules:

$$\text{In−P−In} + 2\text{H}_2\text{O} \rightarrow \text{In−O−P−O−In} + 2\text{H}_2 \quad (3)$$

An In−O−P bridge configuration was already considered in calculations[10] (surface site #12 in their notation) and regarded as one of the configurations with lower formation energy, albeit not the lowest. A similar adsorption mechanism releasing gaseous H_2 was also proposed for Ga-rich GaP(100),[11] but experimentally a mixture of hydroxyl groups and molecularly coadsorbed water was found.[17] For In-rich InP, on the other hand, no further persistent adsorption (at room temperature in UHV) of molecular water seems to take place after all energetically favorable surface sites are occupied. Computationally, Wood et al. predict the reversed behavior with InP favoring molecular and for GaP dissociative adsorption on the pristine surface.[12] If the surface is modified by a submonolayer oxide, however, they predict a stabilization toward dissociative water adsorption because of a higher proton affinity of the oxygen-modified surface.

Oxygen exhibits a higher tendency to directly attack the In−In bonds forming In−O−In bridge topologies. XPS and UPS findings suggest that in addition the oxygen is also present near the phosphorus. The increased density of oxygen on the surface corresponds to roughly half a monolayer. Oxygen also has a tendency to attack the backbonds of the In atoms, modifying, in contrast to H_2O, the surface-modified bulk transition $E_0^{\prime}$. Therefore, here a reaction could be

$$\text{In−In} + \text{P−In} + \text{O}_2 \rightarrow \text{In−O−In} + \text{P−O−In} \quad (4)$$

In the context of solar water splitting, the initial interaction of the In-rich surface with H_2O is actually very favorable. First, the adsorption of water is dissociative, which benefits water splitting kinetically. Second, the released oxygen does not attack the backbonds of the semiconductor surface, which is beneficial for stability. In−O−In bridges, acting as charge carrier traps,[10] appear to be less favorable than In−O−P. These findings could explain the high stability of initially In-rich InP photocathodes under working conditions.[8,9] As the In-rich surface is less stable toward oxygen exposure, the further processing of the surfaces, such as catalyst deposition, should be performed in situ. Ideally, in situ electrochemical functionalization in inert gas atmosphere, as was used earlier for PES characterization,[44] should be combined with a direct, contaminanation-free transfer from growth ambient. Such an approach would allow in situ electrochemical treatments that result in the formation of intermediate films of $InPO_x$ nature which exhibit a sharp interface toward the underlying InP substrate.

For the P-rich surface, no computational studies exist so far. The water molecule appears to efficiently attack here the P-dimer, leading first to a greatly reduced surface ordering induced by the breaking of the P−P bonds and a formation of different oxygen species such as oxides and phosphates at the surface. Annealing in hydrogen ambient leads to a preferential desorption of these weakened phosphorus atoms, possibly in the form of PH_3, similar to water exposure on cleaved InP(110) surfaces,[14] transforming the surface toward some In-rich configuration. The point of attack for persistent oxygen insertion into the surface is again the In−P bond, which exhibits a bond geometry similar to site D of the In-rich surface.

Oxygen exposure, on the other hand, incorporates to a higher degree into the surface, but its impact on surface ordering is, apart from a potential removal of the H atom from the P dimer, less pronounced. A point of attack for the oxygen is again the bond between the first-layer P atom and the second-layer In atom. Also, a higher fraction of the P-dimers is modified toward a P−O−P configuration.

5. CONCLUSION

In summary, we have explored the initial interaction of water and oxygen with atomically well-defined surfaces of InP(100) by complementary spectroscopic methods, probing the predictions of earlier computational studies.[5,10−12] Bridging the so-called "temperature-gap" by conducting our experiments at room temperature, our findings help to improve the microscopic understanding of InP in contact with water and advance the use of reflection anisotropy spectroscopy further towards an in situ study of III−V surface chemistry.

The mixed-dimer In-rich and the P-rich surfaces exhibit a significantly different behavior regarding reactivity toward oxygen and water exposure as well as the degree of reversibility. Both surfaces show a completely dissociative water adsorption, without the formation of persistent hydroxyl groups. This means that in a two-step adsorption process, where hydroxyl groups are most probably an intermediate species, gaseous hydrogen is released. Water adsorption mainly features the formation of In−O−P bonds and only to a small extent the unfavorable, charge-trapping In−O−In bonds. Exposure to molecular oxygen, in contrast, shows a higher tendency to form In−O−In bonds as well as a tendency to diffuse toward the bulk. The surface oxide formation for the In-rich surface after water exposure is highly reversible, as demonstrated by thermal annealing to modest temperatures. Avoiding charge carrier trapping bond geometries and the attack of backbonds could be one of the reasons for the good water-splitting performance and stability of initially In-rich grown InP(100) photocathodes.[8,9] The formation of a small fraction of In−O−In bonds could be the reason for surface recombination, which was found to be still present under working conditions.

From a perspective of device design, our findings suggest that the preparation of well-defined In-rich surfaces can benefit stability and efficiency in InP semiconductor-based photoelectrodes. In a potential tandem structure for unassisted water splitting, the photovoltage provided by optimized InP samples of 0.7−0.8 V allows the use of photoanodes that provide about 1 V at open circuit. An efficient use of the solar spectrum, however, would require the second absorber to exhibit a band gap in the range of 1.6 to 2 eV,[9] such as $Ga_{1-x}In_xP$ protected by a suitable ALD layer. As such an absorber could generate more photovoltage than required for unassisted water-splitting, the device design could relax the requirements for single components as the OER catalyst.

■ ASSOCIATED CONTENT

Supporting Information

XPS overview spectrum of an In-rich surface after water exposure; high-resolution XP spectra around the O 1s region of In-rich surfaces after water (oxygen) exposure and after

dx.doi.org/10.1021/jp502955m | J. Phys. Chem. C 2014, 118, 19032−19041

annealing. This material is available free of charge via the Internet at http://pubs.acs.org.

AUTHOR INFORMATION

Corresponding Author

*E-mail: Matthias.May@helmholtz-berlin.de. Phone:+49(0) 308062-42538.

Notes

The authors declare no competing financial interest.

ACKNOWLEDGMENTS

M.M.M. acknowledges Studienstiftung des deutschen Volkes for his scholarship. This material is based upon work performed by the Joint Center for Artificial Photosynthesis, a DOE Energy Innovation Hub, as follows: parts of the organization of the work, of the discussion, as well as of the manuscript wording and composition were supported through the Office of Science of the U.S. Department of Energy under Award DE-SC0004993.

REFERENCES

(1) Parkinson, B.; Turner, J. The Potential Contribution of Photoelectrochemistry in the Global Energy Future. In *Photoelectrochemical Water Splitting: Materials, Processes and Architectures*; Lewerenz, H.-J., Peter, L., Eds.; The Royal Society of Chemistry: Cambridge, U.K., 2013; Chapter 1, pp 1−18.

(2) Olah, G. A.; Prakash, G. K. S.; Goeppert, A. Anthropogenic Chemical Carbon Cycle for a Sustainable Future. *J. Am. Chem. Soc.* **2011**, *133*, 12881−12898.

(3) Khaselev, O.; Turner, J. A. A Monolithic Photovoltaic-Photoelectrochemical Device for Hydrogen Production via Water Splitting. *Science* **1998**, *280*, 425−427.

(4) Khaselev, O.; Turner, J. A. Electrochemical Stability of p-$GaInP_2$ in Aqueous Electrolytes Toward Photoelectrochemical Water Splitting. *J. Electrochem. Soc.* **1998**, *145*, 3335−3339.

(5) Wood, B. C.; Schwegler, E.; Choi, W. I.; Ogitsu, T. Hydrogen-Bond Dynamics of Water at the Interface with InP/GaP(001) and the Implications for Photoelectrochemistry. *J. Am. Chem. Soc.* **2013**, *135*, 15774−15783.

(6) Fujishima, A.; Honda, K. Electrochemical Photolysis of Water at a Semiconductor Electrode. *Nature (London, U.K.)* **1972**, *238*, 37−38.

(7) Kaiser, B.; Fertig, D.; Ziegler, J.; Klett, J.; Hoch, S.; Jaegermann, W. Solar Hydrogen Generation with Wide-Band-Gap Semiconductors: GaP(100) Photoelectrodes and Surface Modification. *ChemPhysChem* **2012**, *13*, 3053−3060.

(8) Lewerenz, H. J.; Heine, C.; Skorupska, K.; Szabo, N.; Hannappel, T.; Vo-Dinh, T.; Campbell, S. A.; Klemm, H. W.; Muñoz, A. G. Photoelectrocatalysis: Principles, Nanoemitter Applications and Routes to Bio-Inspired Systems. *Energy Environ. Sci.* **2010**, *3*, 748.

(9) Hannappel, T.; May, M. M.; Lewerenz, H.-J. Epitaxial III-V Thin Film Absorbers: Preparation, Efficient InP Photocathodes and Routes to High Efficiency Tandem Structures. In *Photoelectrochemical Water Splitting: Materials, Processes and Architectures*; Lewerenz, H.-J., Peter, L., Eds.; The Royal Society of Chemistry: Cambridge, U.K., 2013; Chapter 9, pp 223−265.

(10) Wood, B. C.; Ogitsu, T.; Schwegler, E. Local Structural Models of Complex Oxygen- and Hydroxyl-Rich GaP/InP(001) Surfaces. *J. Chem. Phys.* **2012**, *136*, 064705-1−064705-11.

(11) Jeon, S.; Kim, H.; Goddard, W. A.; Atwater, H. A. DFT Study of Water Adsorption and Decomposition on a Ga-Rich GaP(001)(2 × 4) Surface. *J. Phys. Chem. C* **2012**, *116*, 17604−17612.

(12) Wood, B. C.; Schwegler, E.; Choi, W. I.; Ogitsu, T. Surface Chemistry of GaP(001) and InP(001) in Contact with Water. *J. Phys. Chem. C* **2014**, *118*, 1062−1070.

(13) Webb, C.; Lichtensteiger, M. Formation of Alternative Surface Oxide Phases on GaAs by Adsorption of O_2 or H_2O: A UPS, XPS, and SIMS Study. *J. Vac. Sci. Technol. (N.Y., NY, U.S.)* **1982**, *21*, 659−662.

(14) Henrion, O.; Klein, A.; Jaegermann, W. Water Adsorption on UHV Cleaved InP(110) Surfaces. *Surf. Sci.* **2000**, *457*, L337−L341.

(15) Chen, G.; Visbeck, S. B.; Law, D. C.; Hicks, R. F. Structure-Sensitive Oxidation of the Indium Phosphide (001) Surface. *J. Appl. Phys.* **2002**, *91*, 9362−9367.

(16) May, M. M.; Supplie, O.; Höhn, C.; Zabka, W.-D.; Lewerenz, H.-J.; van de Krol, R.; Hannappel, T. Water-Induced Modifications of GaP(100) and InP(100) Surfaces Studied by Photoelectron Spectroscopy and Reflection Anisotropy Spectroscopy. *Proc. SPIE* **2013**, *8822*, 88220M-1−88220M-7.

(17) May, M. M.; Supplie, O.; Höhn, C.; van de Krol, R.; Lewerenz, H.-J.; Hannappel, T. The Interface of GaP(100) and H_2O Studied by Photoemission and Reflection Anisotropy Spectroscopy. *New J. Phys.* **2013**, *15*, 103003.

(18) Zhang, X.; Ptasinska, S. Dissociative Adsorption of Water on an H_2O/GaAs(100) Interface: In Situ Near-Ambient Pressure XPS Studies. *J. Phys. Chem. C* **2014**, *118*, 4259−4266.

(19) Schmidt, W. G.; Esser, N.; Frisch, A. M.; Vogt, P.; Bernholc, J.; Bechstedt, F.; Zorn, M.; Hannappel, T.; Visbeck, S.; Willig, F.; Richter, W. Understanding Reflectance Anisotropy: Surface-State Signatures and Bulk-Related Features in the Optical Spectrum of InP(001)(2 × 4). *Phys. Rev. B: Condens. Matter Mater. Phys.* **2000**, *61*, R16335−R16338.

(20) Schmidt, W. G.; Hahn, P. H.; Bechstedt, F.; Esser, N.; Vogt, P.; Wange, A.; Richter, W. InP(001)-(2 × 1) Surface: A Hydrogen Stabilized Structure. *Phys. Rev. Lett.* **2003**, *90*, 126101.

(21) Witkowski, N.; Coustel, R.; Pluchery, O.; Borensztein, Y. RAS: An Efficient Probe to Characterize Si(001)-(2 × 1) Surfaces. *Surf. Sci.* **2006**, *600*, 5142−5149.

(22) Hannappel, T.; Töben, L.; Möller, K.; Willig, F. In-Situ Monitoring of InP(100) and GaP(100) Interfaces and Characterization with RDS at 20 K. *J. Electron. Mater.* **2001**, *30*, 1425−1428.

(23) Smith, C. I.; Bowfield, A.; Dolan, G. J.; Cuquerella, M. C.; Mansley, C. P.; Fernig, D. G.; Edwards, C.; Weightman, P. Determination of the Structure of Adenine Monolayers Adsorbed at Au(110)/Electrolyte Interfaces Using Reflection Anisotropy Spectroscopy. *J. Chem. Phys.* **2009**, *130*, 044702−044702−9.

(24) Haberland, K.; Kurpas, P.; Pristovsek, M.; Zettler, J.-T.; Weyers, M.; Richter, W. Spectroscopic Process Sensors in MOVPE Device Production. *Appl. Phys. A: Mater. Sci. Process.* **1999**, *68*, 309−313.

(25) Visbeck, S.; Hannappel, T.; Zorn, M.; Zettler, J.; Willig, F. Temperature Dependence and Origin of InP(100) Reflectance Anisotropy Down to 20 K. *Phys. Rev. B: Condens. Matter Mater. Phys.* **2001**, *63*, 245303.

(26) Letzig, T.; Schimper, H.-J.; Hannappel, T.; Willig, F. P-H Bonds in the Surface Unit Cell of P-rich Ordered InP(001) Grown by Metalorganic Chemical Vapor Deposition. *Phys. Rev. B: Condens. Matter Mater. Phys.* **2005**, *71*, 033308.

(27) Hannappel, T.; Visbeck, S.; Töben, L.; Willig, F. Apparatus for Investigating Metalorganic Chemical Vapor Deposition-Grown Semiconductors with Ultrahigh-Vacuum Based Techniques. *Rev. Sci. Instrum.* **2004**, *75*, 1297.

(28) Schmidt, W. G.; Bechstedt, F. Geometry and Electronic Structure of InP(001)(2 × 4) Reconstructions. *Surf. Sci.* **1998**, *409*, 474−484.

(29) Schmidt, W. G.; Briggs, E. L.; Bernholc, J.; Bechstedt, F. Structural Fingerprints in the Reflectance Anisotropy Spectra of InP(001)(2 × 4) Surfaces. *Phys. Rev. B: Condens. Matter Mater. Phys.* **1999**, *59*, 2234.

(30) Schmidt, W. G.; Bechstedt, F.; Bernholc, J. Understanding Reflectance Anisotropy: Surface-State Signatures and Bulk-Related Features. *J. Vac. Sci. Technol., B* **2000**, *18*, 2215.

(31) Hannappel, T.; Töben, L.; Visbeck, S.; Crawack, H. J.; Pettenkofer, C.; Willig, F. UPS and 20 K Reflectance Anisotropy Spectroscopy of the P-rich and In-rich Surfaces of InP(1 0 0). *Surf. Sci.* **2000**, *470*, L1−L6.

(32) Hannappel, T.; Visbeck, S.; Zorn, M.; Zettler, J.-T.; Willig, F. Reflectance Anisotropy Spectra for the Transition from the P-rich to the In-rich Surface Reconstruction of InP(100). *J. Cryst. Growth* **2000**, *221*, 124−128.
(33) Lautenschlager, P.; Garriga, M.; Cardona, M. Temperature Dependence of the Interband Critical-Point Parameters of InP. *Phys. Rev. B: Condens. Matter Mater. Phys.* **1987**, *36*, 4813−4820.
(34) Acosta-Ortiz, S. E.; Lastras-Martínez, A. Electro-Optic Effects in the Optical Anisotropies of (001) GaAs. *Phys. Rev. B: Condens. Matter Mater. Phys.* **1989**, *40*, 1426−1429.
(35) Wojdyr, M. *Fityk*: A General-Purpose Peak Fitting Program. *J. Appl. Crystallogr.* **2010**, *43*, 1126−1128.
(36) Janowitz, C.; Scherer, V.; Mohamed, M.; Krapf, A.; Dwelk, H.; Manzke, R.; Galazka, Z.; Uecker, R.; Irmscher, K.; Fornari, R.; et al. Experimental Electronic Structure of In_2O_3 and Ga_2O_3. *New J. Phys.* **2011**, *13*, 085014.
(37) Henderson, M. A. The Interaction of Water with Solid Surfaces: Fundamental Aspects Revisited. *Surf. Sci. Rep.* **2002**, *46*, 1−308.
(38) Fadley, C. S. Angle-Resolved X-Ray Photoelectron Spectroscopy. *Prog. Surf. Sci.* **1984**, *16*, 275−388.
(39) Powell, C.; Jablonski, A. NIST Electron Effective-Attenuation-Length Database, Version 1.3, Standard Reference Data Program Database 82, National Institute of Standards and Technology: Gaithersburg, MD, 2011; http://www.nist.gov/srd/nist82.cfm.
(40) Coe, J. V.; Earhart, A. D.; Cohen, M. H.; Hoffman, G. J.; Sarkas, H. W.; Bowen, K. H. Using Cluster Studies to Approach the Electronic Structure of Bulk Water: Reassessing the Vacuum Level, Conduction Band Edge, and Band Gap of Water. *J. Chem. Phys.* **1997**, *107*, 6023−6031.
(41) Yeh, J.; Lindau, I. Atomic Subshell Photoionization Cross Sections and Asymmetry Parameters: $1 < Z < 103$. *At. Data Nucl. Data Tables* **1985**, *32*, 1−155.
(42) Farrow, R. F. C. The Evaporation of InP under Knudsen (Equilibrium) and Langmuir (Free) Evaporation Conditions. *J. Phys. D: Appl. Phys.* **1974**, *7*, 2436.
(43) Foxon, C. T.; Joyce, B. A.; Farrow, R. F. C.; Griffiths, R. M. The Identification of Species Evolved in the Evaporation of III-V Compounds. *J. Phys. D: Appl. Phys.* **1974**, *7*, 2422.
(44) Lewerenz, H.; Schulte, K. Combined Photoelectrochemical Conditioning and Surface Analysis of InP Photocathodes: II. Photoelectron Spectroscopy. *Electrochim. Acta* **2002**, *47*, 2639−2651.
(45) Lundholm, M.; Siegbahn, H.; Holmberg, S.; Arbman, M. Core Electron Spectroscopy of Water Solutions. *J. Electron Spectrosc. Relat. Phenom.* **1986**, *40*, 163−180.